RESEARCH ARTICLE | AUGUST 13 2024

Deeper-band electron contributions to stopping power of silicon for low-energy ions *⊙*

F. Matias 🗷 📵 ; P. L. Grande 📵 ; N. E. Koval 📵 ; J. M. B. Shorto 📵 ; T. F. Silva 📵 ; N. R. Arista 📵



J. Chem. Phys. 161, 064310 (2024) https://doi.org/10.1063/5.0218226





Articles You May Be Interested In

Which triatomic monohalosilylenes, monohalogermylenes, and monohalostannylenes (HMX) fluoresce or phosphoresce and why? An *ab initio* investigation

J. Chem. Phys. (February 2022)

Tight-binding analysis of helical states in carbyne

J. Chem. Phys. (September 2020)

van der Waals density functionals built upon the electron-gas tradition: Facing the challenge of competing interactions

J. Chem. Phys. (April 2014)





Deeper-band electron contributions to stopping power of silicon for low-energy ions

Cite as: J. Chem. Phys. 161, 064310 (2024); doi: 10.1063/5.0218226

Submitted: 9 May 2024 • Accepted: 24 July 2024 •

Published Online: 13 August 2024



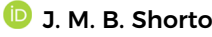


















AFFILIATIONS

- ¹ Instituto de Pesquisas Energéticas e Nucleares, Av. Professor Lineu Prestes, São Paulo 05508-000, Brazil
- ²Instituto de Física da Universidade Federal do Rio Grande do Sul, Av. Bento Gonçalves, Porto Alegre 9500, Brazil
- ³Centro de Física de Materiales, Paseo Manuel de Lardizabal 5, Donostia-San Sebastián 20018, Spain
- ⁴Instituto de Física da Universidade de São Paulo, Rua do Matão, Trav. R187, São Paulo 05508-090, Brazil
- ⁵ División Colisiones Atómicas, Instituto Balseiro, Centro Atómico Bariloche, and Comisión Nacional de Energía Atómica, Bariloche 8400, Argentina

ABSTRACT

This study provides accurate results for the electronic stopping cross sections of H, He, N, and Ne in silicon in low to intermediate energy ranges using various non-perturbative theoretical methods, including real-time time-dependent density functional theory, transport cross section, and induced-density approach. Recent experimental findings [Ntemou et al., Phys. Rev. B 107, 155145 (2023)] revealed discrepancies between the estimates of density functional theory and the observed values. We show that these discrepancies vanish by considering the nonuniform electron density of the deeper silicon bands for ion velocities approaching zero ($\nu \to 0$). This indicates that mechanisms such as "elevator" and "promotion," which can dynamically excite deeper-band electrons, are active, enabling a localized free-electron gas to emulate ion energy loss, as pointed out by Lim et al. [Phys. Rev. Lett. 116, 043201 (2016)]. The observation and the description of a velocityproportionality breakdown in electronic stopping cross sections at very low velocities are considered to be a signature of the contributions of deeper-band electrons.

Published under an exclusive license by AIP Publishing. https://doi.org/10.1063/5.0218226

I. INTRODUCTION

Recent studies on the interaction of various ions with solids in the low- and intermediate-energy ranges provide new and relevant insights into various aspects of the interaction process, including important nonlinear and band-structure effects. 1-9 In particular, recent experimental studies on the stopping power of light and heavy ions in TiN and Si targets ^{10,11} have reported significant discrepancies in electronic stopping cross sections compared to the standard estimates of density functional theory (DFT). 12,13 The reported effect strongly enhances the experimental values relative to the DFT predictions (assuming uniform electron density conditions). 10,11 In a previous study, 14 we provided quantitative analysis of the experimental results reported in Ref. 10 for TiN using two alternative theoretical frameworks, namely, (i) a self-consistent model for a nonuniform electron gas together with quantum scattering and transport cross section (TCS) calculations and (ii) a Penn-type

ensemble of electrons also using TCS calculations. It is important to note that in both non-perturbative methods, a nonlinear description of the interaction between incident ions and target electrons was applied.

In the present study, we extend the previous theoretical analysis to the most recent experiments on Si targets, 11 showing that these results can be quantitatively described using the theoretical approach previously proposed.¹⁴ In this study, we extend the methodology described in Ref. 14, incorporating the induceddensity approach (IDA) and real-time time-dependent density functional theory (TDDFT) to calculate the local electronic stopping

In the IDA, the stopping force (or stopping power) is calculated based on the electron density that is induced in the medium due to the presence of the moving charged particle. This displaced electron density creates a space charge and, thus, a force on the projectile, namely, the stopping force. Traditionally, the response

a) Author to whom correspondence should be addressed: phdflaviomatias@gmail.com

of the electron gas (or electron density) to the perturbation caused by the moving charged particle has been treated linearly. However, a recently developed formula allows for non-linear calculations, although it applies to central electron–ion potentials.^{7,8}

Real-time TDDFT is a state-of-the-art methodology for calculating non-perturbative electronic stopping power. However, applying real-time TDDFT to atomistic models can be computationally demanding. Multiple trajectories must be considered to accurately sample all possible electron-density regions to obtain a random (or average) stopping power. ^{15,16} Moreover, heavy projectile descriptions require the explicit inclusion of core electrons, which play a significant role in the projectile's energy loss. ⁹ Real-time TDDFT applied to a uniform electron gas is more computationally efficient; however, it is more suitable for free electron metals. To describe more complex targets, one has to account for density nonuniformities.

Combining real-time TDDFT with the Penn model has successfully predicted the electronic stopping power of various targets with high accuracy.¹⁷ Such an approach incorporates the efficiency and accuracy of real-time TDDFT for a nearly uniform electron gas, with the Penn approach describing the electron density in different regions of the target material.

Thus, in this work, we employ three methods for calculating the electronic stopping power, namely, the real-time TDDFT (an *ab initio* method), TCS (based on the transport theory), and IDA (an analytical method). Each method has unique advantages and limitations, which we leverage for a comprehensive analysis and comparison. All the three methods are combined with two different ways of describing the nonuniform electron density in the target. The first is the local-density approximation (LDA) based on the Lindhard theory, which assumes a locally uniform electron gas. The second method is the Penn algorithm, which uses optical data to derive an energy-loss function and employs the dielectric function to describe the electron density. A detailed description of the LDA and Penn models and the combination of those with the real-time TDDFT, TCS, and IDA methods to calculate the electronic stopping power is provided in Sec. II.

Atomic units (a.u., $e = m_e = \hbar = 1$) are used throughout the text unless otherwise stated.

II. THEORETICAL PROCEDURES

The theoretical formulation contains some important physical ingredients, as follows:

(1) Nonlinear screening (Friedel sum rule): the interaction of slow ions with solids requires a quantum mechanical analysis even for light ions, such as H and He; ^{12,13} the nonlinear character of the electron–ion interactions becomes increasingly relevant for heavier ions. ^{13,14} DFT provides a useful tool for accurately describing the interaction of target electrons with intruder ions. ^{12,13} An alternative method, first used by Ferrell and Ritchie¹⁸ and followed by Cherubini and Ventura¹⁹ and Apagy and Nagy, ²⁰ consists of using analytical models for the screening potential, which contain a screening parameter whose value is adjusted self-consistently using the so-called Friedel sum rule (FSR). ^{21,22} This rule was originally derived for the case of static impurities in a free

- electron gas (FEG); an extension of this rule for the case of moving ions was obtained later. 23 The extended FSR was applied to light and heavy ions in an extended range of velocities, showing excellent agreement with the experimental values. $^{24-26}$
- Local density approximation (LDA) describes the nonuniform electron density in the target for calculating electronic stopping power (not to be confused with the local density approximation used in density functional theory to describe exchange-correlation effects). This approximation is longstanding, following a set of pioneering studies by Lindhard and Scharff, 27-29 who obtained very good agreement with the experimental values of stopping powers and energy straggling for protons and helium ions in solid targets. Using the LDA method, Rousseau et al. 30 successfully explained the oscillatory dependence of the stopping cross section (SCS) of alpha particles with the target atomic number Z_2 . These studies were performed for intermediate- and high-energy ranges, where linearized models are applied. However, the case of slow heavy ions in solids is a much more complex problem. Using a combination of FSR with LDA, Calera-Rubio et al.³¹ provided a consistent description of the oscillatory dependence of the stopping power on the atomic number of ions Z_1 . An important difference between the latter work and the previous ones is that the calculation of Ref. 31 applies in the non-perturbative range where quantum cross-section analysis must be considered. In contrast, previous studies^{27,30} relate to the range of linearized models.
- (3) Penn algorithm: Penn³² introduced an algorithm to determine the inelastic mean free paths (IMFP) of electrons employing a model dielectric function. This function can be derived from the experimental optical data of the specific material under investigation, utilizing the Lindhard model dielectric function and considering various plasmon energies or electron densities. Furthermore, the same model has been used to estimate the stopping power of electrons in different materials³³ and extended to calculate the nonlinear stopping power of ions.³⁴ This extension involves using the energy loss function (ELF) to weigh the contributions of different components of the electron gas within a statistical ensemble that characterizes the material of interest.

In this work, we combine the LDA and Penn algorithms for describing nonlocal electron density with three non-perturbative methods for calculating the electronic stopping power, namely, real-time TDDFT, TCS, and IDA, as described in the following.

A. Real-time TDDFT-, TCS-, and IDA-LDA approaches

The first approach considered here is based on the method proposed in Ref. 14, which consists of using the LDA method to describe the nonuniform electron density in the Si target, together with nonlinear calculations of the energy loss of ions in a uniform (locally) electron gas. The target is described by its local density values n(r) or equivalently local $r_s(r)$ values, related by $1/n(r) = (4\pi/3)r_s^3$.

For calculations using the LDA method, prior knowledge of the electronic density of the Si target is necessary. In this paper, the theoretical electron density of Si was extracted from the Ziegler tables.³⁵ The atomic density of Si is $\rho = 2.33$ g/cm³. For the sake of reliability,

we analyzed the normalization of the electron density to the number of electrons in the Si atom, calculated as

$$N_e = 4\pi \int_0^{r_{\text{cell}}} n(r) r^2 dr. \tag{1}$$

Equation (1) was applied by assuming an atomic Wigner–Seitz sphere (WS) around the atom of Si. The solution of this equation was obtained by integrating until the radius of the atomic cell $r_{\rm cell} = 3.195$ a.u. (vertical dashed violet line), resulting in 14.017 electrons

In this approach, the final step is to integrate the stopping powers over the WS cells corresponding to the Si atom using the following expression:

$$\left[\frac{dE}{dz}(v)\right]_{X-LDA} = 4\pi N_a \int_0^\infty r^2 dr \left[\frac{dE}{dz}(v)\right]_X (v, r_s(r)), \qquad (2)$$

where $N_a = 1/V_a$ is the number of Si atom per unit volume: $V_a = (4\pi/3)r_{\text{cell}}^3$. In Eq. (2), X = TDDFT, TCS, or IDA. The values of $r_s(r)$ are shown in Fig. 1.

Figure 1 shows the electron density in relation to the radial distance r from the Si nuclei (blue dashed line) and the r_s (r) values (red dashed–double-dotted line).

The theoretical electron density multiplied by $4\pi r^2$ as a function of the atomic cell radii of Si is shown in Fig. 2 (solid line). The vertical solid lines represent the integration ranges for the calculations converged of Eq. (2). The knowledge of these intervals was obtained from the convergence of Eq. (2) in $\nu = 0.1$ a.u. These ranges correspond to the electrons that effectively contribute to the electron–projectile interaction, namely, 6 electrons for H⁰ (0.65–3.195 a.u.), 10 for He⁰ (0.35–3.195 a.u.), and 12 electrons for N⁰ and Ne⁰ (0.17–3.195 a.u.). We also show the radial interval corresponding to 4.2 electrons, in analogy to the uniform FEG (4.2 electrons) with the experimental density parameter, $r_{\rm s,exp} = 1.97~{\rm a.u.}^{36}$

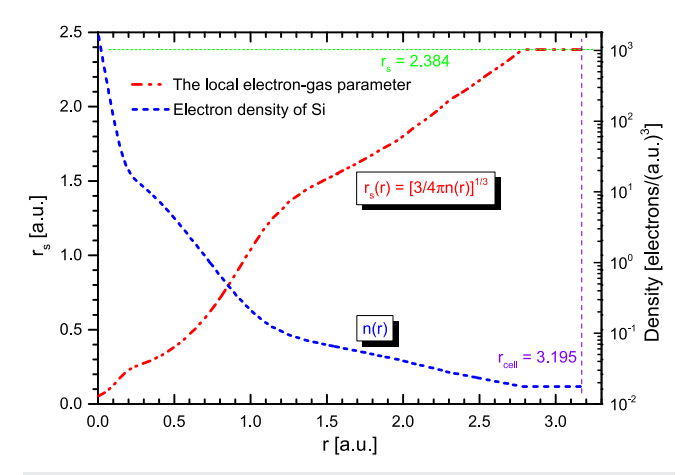


FIG. 1. Radial electron density (blue dashed line) within the WS sphere encompassing the Si atom. The radial distance $r_{\rm cell}=3.195$ a.u. represents the atomic cell radius of Si. The values of the local electron-gas parameter $r_{\rm s}$ are shown by a red dashed–double-dotted line. At the cell boundary, $r_{\rm s}=2.384$ a.u.

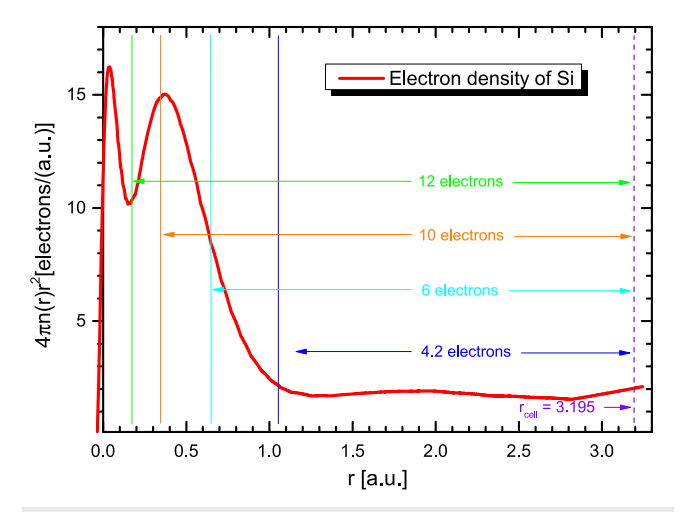


FIG. 2. Electron density multiplied by $4\pi r^2$ as a function of the atomic cell radii of Si. The spacing between each solid vertical line and the dashed vertical line (atomic cell radius of Si, r_{cell}) indicates the number of electrons that effectively contribute to the nonuniform FEG in electron–projectiles interaction, namely, six for H⁰, eight for He⁰, and ten for N⁰ and Ne⁰. We also show the radial interval corresponding to 4.2 electrons (nonuniform FEG), in analogy to the uniform FEG (4.2 electrons) with the experimental density parameter, $r_{s,\text{exp}} = 1.97$ a.u.³⁶

B. Real-time TDDFT-, TCS-, and IDA-Penn approaches

Recently, a new non-perturbative method has been introduced to characterize the electronic stopping power of light and heavy ions in materials. The Penn approach has been successfully utilized in the TCS for low-energy protons with velocities lower than the Fermi velocity ($\nu < \nu_F$, the concept used for metals to define the electron velocity at the Fermi surface, here used to express the velocity relation to the electron–gas parameter r_s : $\nu_F = 1.919/r_s$ a.u.). This approach has been successfully applied to predict the accurate electronic stopping power of protons in polymers using real-time TDDFT over a wide range of proton energies (0.25–10000 keV). This method considers the combination of electron gas responses characterized by nonuniform densities. It is similar to the approach outlined in the Penn method. To analyze each free-electron density, the ELF of the material is used at the optical limit,

$$g(\omega_{\rm p}) = \frac{2}{\pi \omega_{\rm p}} \, \text{ELF}(\omega_{\rm p}).$$
 (3)

Figure 3 shows the optical-ELF data of Si, as presented in Ref. 37. As discussed later, these ranges correspond to the deeper- and valence-band electrons that effectively contribute to the electron–projectiles interaction, namely, 9 electrons for H⁰ and H⁺ (0.32–260) eV, 12 for He⁰ (0.32–1000) eV, 13.3 for N⁰ (0.32–2700) eV, and 13.7 electrons for Ne⁰ (0.32–3600) eV. As shown in Fig. 2, we also show the experimental valence band range (0.32–100) eV corresponding to 4.2 electrons, analogously to the uniform FEG (4.2 electrons), with these, the density parameter $r_{\rm s,exp}=1.97$ a.u., a value calculated from the experimental plasmon energy, $\omega_{\rm p,exp}=17$ eV.³⁶ The sum rule³⁴ gives 14 electrons with the full ELF (0.32–5000) eV.

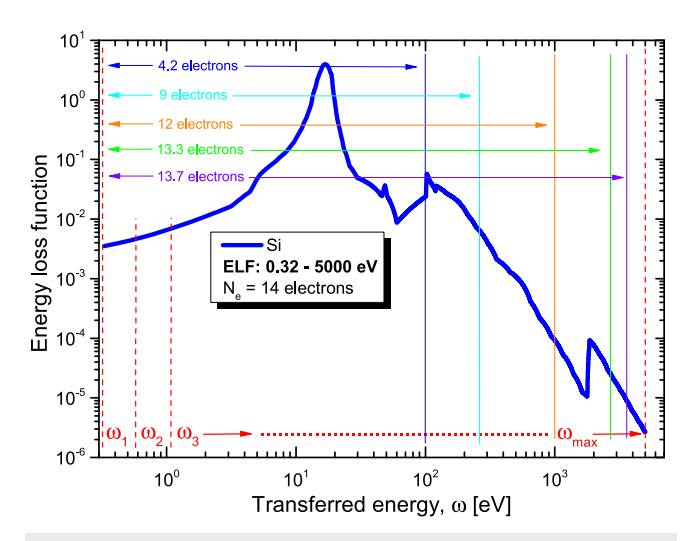


FIG. 3. Optical-ELF data for Si obtained from Ref. 37. The spacing between each solid vertical line and the dashed vertical line ($\omega_1=0.32$ eV) indicates the number of electrons that effectively contribute to the nonuniform FEG in the electron–projectile interaction, namely, 9 for H⁰ and H⁺, 12 for He⁰, 13.3 for N⁰, and 13.7 for Ne⁰. These ranges correspond to the convergent values of stopping power obtained using Eq. (8) in $\nu=0.1$ a.u. We also show the valence band range (0.32–100) eV corresponding to 4.2 electrons (nonuniform FEG), in analogy to the uniform FEG (4.2 electrons) with the experimental density parameter, $r_{\rm s,exp}=1.97$ a.u.³⁶ The intervals from ω_1 to $\omega_{\rm max}$ yield 14 electrons from applying the sum rule.³⁴

The stopping power depends on the plasmon energy $\omega_{\rm p}$ determined by the contributions of individual electron gases obtained from $r_{\rm s}$: $\omega_{\rm p} = \sqrt{3} r_{\rm s}^{-3/2}$. Hence, the method for calculating the stopping power is as follows:

$$\left[\frac{dE}{dz}(v)\right]_{X-Penn} = \int_0^\infty d\omega_p g(\omega_p) \left[\frac{dE}{dz}(v)\right]_X(v,\omega_p), \qquad (4)$$

where X \equiv TDDFT, TCS, or IDA; the electronic stopping $\left[\frac{dE}{dz}(v)\right]_{\rm X}$ is given by Eqs. (6) and (8), respectively (see Secs. II C and II D). Due to their unique characteristics, we have named these approaches TDDFT-Penn, TCS-Penn, and IDA-Penn.

C. Real-time TDDFT method

Real-time TDDFT is a highly accurate tool *ab initio* to describe electronic stopping power in spherical jelliums. The jellium model assumes a positive background (representing the ion cores) that provides a charge balancing for the electron gas. Compared to fully atomistic models, the advantage of jellium representation is the computational efficiency. Real-time TDDFT in an FEG has shown accurate results for near-free-electron systems.

The approach adopted in this work reflects the methodology used in Refs. 2, 8, and 38–43 and will be briefly explained in this section. In this approach, the time evolution of the electron density incorporates, in a non-perturbative manner, the complete dynamic interaction between an external field and the medium. This computational framework has been used to analyze various issues in condensed matter systems, such as dynamic charge screening in metallic

media,⁴⁴ energy loss of atomic particles in matter,^{2,8} and many-body effects associated with hole screening in photoemission.⁴²

A static density functional theory (DFT) calculation is performed to obtain the system's ground state. The time evolution of the complete electron density, $n(\mathbf{r},t)$, in response to an external field (in this case, a proton) is conducted within the framework of real-time TDDFT in the Kohn–Sham scheme. The moving ion is modeled as a bare Coulomb charge, i.e., an external Coulomb potential in the time-dependent Kohn–Sham equations (see the details in work of Koyal *et al.*⁴³).

The energy loss is calculated by integrating the time-dependent induced force F over the proton,

$$E_{\text{loss}}(\nu) = -\nu \int_{-\infty}^{+\infty} F(t)dt,$$
 (5)

where ν is the (constant) velocity at which the proton traverses the jellium. Once the induced force on the proton is calculated, the average (or effective) stopping power is computed as the energy loss per unit path length, i.e.,

$$\left[\frac{dE}{dz}(v)\right]_{\text{TDDET}} = \frac{E_{\text{loss}}(v)}{D},\tag{6}$$

where D is the diameter of the jellium sphere.

Real-time TDDFT is applied only to the electronic stopping power calculations for protons in matter because the current code considers only bare ions as projectiles. Extending this method to heavier ions, including charge states in the electron–ion process, requires substantial effort. Therefore, self-consistent methods based on the FSR and analytical screening potentials currently represent the most convenient approach for studying nonlinear effects in the electronic screening charge and energy losses of heavier ions in matter.

D. IDA and TCS methods

Within the framework of stationary states, the electronic stopping power is also calculated using two theoretical models: the TCS²⁴ and the induced-density approach (IDA).^{7,8}

TCS method was first introduced by Finnemann⁴⁵ and was applied by Briggs and Pathak to explain the oscillatory dependence of the stopping power on the atomic number Z_1 for channeled ions with low velocities.⁴⁶ Significant contributions were made by Echenique, Puska, Nieminen, Ashley, and Ritchie following the development of DFT methods.^{12,13} As indicated above, a simplified nonlinear approach was proposed, which uses parametric screening potentials in conjunction with the FSR. The extension of the FSR to finite ion velocities²⁴ opened the way to self-consistent calculations for light and heavy ions in a wide range of velocities.

The calculations of TCS²⁴ and IDA^{7,8} use a model potential with parameter α , as detailed in Ref. 8. Through the numerical integration of the Schrödinger radial equation, the phase shifts of scattering $\delta_{\ell}(\nu)$ were determined for a large number of values ℓ , depending on both the density parameter r_s and the potential parameter α .⁸ The value of α (for each r_s) was determined iteratively to satisfy the FSR,

$$Z = \frac{2}{\pi} \sum_{\ell=0}^{\ell_{\text{max}}} (2\ell + 1) \delta_{\ell}(\nu), \tag{7}$$

requiring multiple iterations for a self-consistent solution. We derived the ultimate phase shift values for each combination of Z, r_s , and ν through an iterative process. The range of the r_s values considered ranged from 0.1 to 2.384 a.u., which covered the relevant range of this study (see Fig. 1). Once we obtained the δ_ℓ values, we used them to calculate the TCS, using the following equation:

$$\left[\frac{dE}{dz}(v)\right]_{X} = n_0 m_e \left(\frac{|\vec{v}_e - \vec{v}|}{v} \vec{v} \cdot (\vec{v} - \vec{v}_e) \sigma_{tr}^{X}(|\vec{v}_e - \vec{v}|)\right)_{\vec{v}_e}, \quad (8)$$

where m_e is the electron mass, $\langle \cdots \rangle_{\vec{v}_e}$ stands for the average over the electron velocities \vec{v}_e , \vec{v} is the ion velocity, n_0 is the undisturbed electron density, σ^X_{tr} is the transport cross section, and $X \equiv IDA$ or TCS. For $X \equiv TCS$, σ^{TCS}_{tr} can be expressed by phase shifts δ_ℓ at the relative speed v', according to Ref. 47,

$$\sigma_{\rm tr}^{\rm TCS}(\nu') = \frac{4\pi}{\nu'^2} \sum_{\ell=0}^{\infty} (\ell+1) \sin^2[\delta_{\ell}(\nu') - \delta_{\ell+1}(\nu')]. \tag{9}$$

For $X \equiv IDA$, the electronic stopping power of ions is estimated by Eq. (8) with the effective transport cross section, according to Ref. 7,

$$\sigma_{\rm tr}^{\rm IDA}(\nu') = \frac{2\pi Z}{\nu'^3} \sum_{\ell=0}^{\infty} \sin(2[\delta_{\ell}(\nu') - \delta_{\ell+1}(\nu')]).$$
 (10)

We highlight that the IDA and TCS methods yield the same results for neutral projectiles. See Refs. 7 and 8 for more details on the IDA model.

III. RESULTS

The results are presented as the electronic stopping cross section (SCS), i.e., the electronic stopping power normalized by the atomic density of the target material.

The electronic SCSs of H, He, N, and Ne in Si are shown in Figs. 4–8. The letters represent the experimental IAEA database. 48 Furthermore, we have included recent data from the Uppsala group, 11 represented by star symbols. In Fig. 4, the black open circle and the cyan diamond symbols represent the experimental data from Japan²⁵ and Bariloche⁴⁹ groups, respectively. The red solid line represents the semi-empirical predictions of SRIM-2013.⁵⁰ The observed anomalies in some SRIM curves are artifacts resulting from overfitting. We employed three non-perturbative methods to compute the SCS of ions: real-time TDDFT, TCS, and IDA, combined with Penn or LDA. The results obtained using Eqs. (2) and (4) are shown in Fig. 4. The results show that for v > 1.0 a.u. (25 keV), the real-time TDDFT-Penn and IDA-Penn approaches are highly similar and are in excellent agreement with the experimental data, especially those from the Uppsala group.¹¹ Nevertheless, for velocities between 2.0 and 3.2 a.u., the real-time TDDFT-Penn approach agrees better with the Uppsala data.

For v < 1.0 a.u., the real-time TDDFT-Penn and the real-time TDDFT-LDA approaches tend to overestimate the stopping power. One plausible explanation for this discrepancy is to consider the inclusion of the neutral H⁰ charge state. In this velocity range, this charge state is predominant. For v < 0.6 a.u., the estimation of the CasP 6.0 program indicates a 100% probability of H⁰ presence. 8,52 The charge state is taken into account in the TCS and IDA calculations as H⁰, while in the real-time TDDFT, the projectile is H⁺.

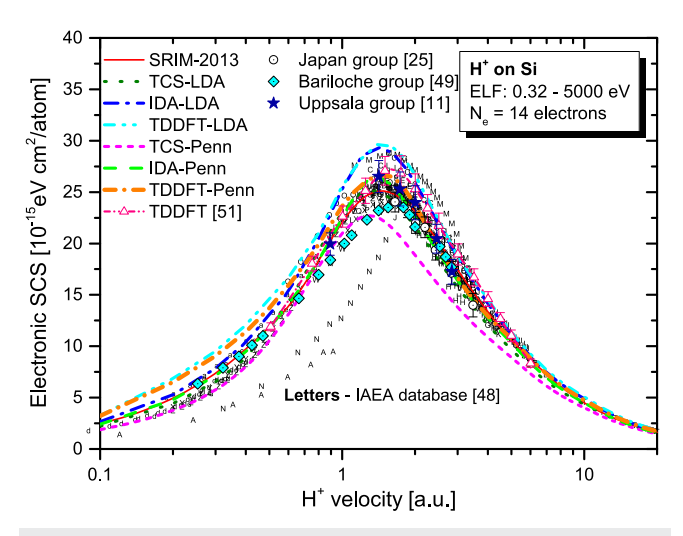


FIG. 4. Electronic SCS for H⁺ ions on Si as a function of velocity. TCS-LDA (olive dotted line), IDA-LDA (blue dashed–dotted line), real-time TDDFT-LDA (cyan dashed–double-dotted line), TCS-Penn (magenta short-dashed line), IDA-Penn (green dashed line), and real-time TDDFT-Penn (orange short-dash–dotted line) results are shown. Our results are compared to those of the semi-empirical SRIM-2013 model (red solid-line),⁵⁰ and experimental data available in the IAEA database (uppercase letters),⁴⁸ Real-time TDDFT results (light-red short-dashed–dotted line with triangles) by Yost *et el.*,⁵¹ scaled to account for the core correction, are also presented. The experimental data from the Japan group (black open circle symbols)²⁵ and the Bariloche group (cyan diamond symbols)⁴⁹ are also shown. The royal star symbols represent recent data from the Uppsala group. ¹¹

Therefore, these observations suggest the importance of considering the appropriate charge state for this velocity range in electronic stopping power calculations.

As observed in Fig. 4, it is evident that the TCS-Penn results are lower than the actual values in the Bragg peak region. At high velocities, the TCS-Penn results slowly converge to the experimental results. This is a fundamental feature of the TCS method, as it does not precisely converge to the Bethe formula, which has been discussed in previous studies.^{7,8}

The results of H⁺ obtained from real-time TDDFT-LDA and IDA-LDA (Fig. 4) show that the LDA tends to overestimate the SCS compared to the average values of the experimental data in the velocity range $v_F < v < 5$ a.u., where $v_F = 1.919/r_s$ a.u. In the LDA approach, the SCS is overestimated throughout the v < 5 a.u. range for He, N, and Ne. For this reason, the results based on the LDA approach are not presented for Z > 1. This overestimation of the stopping power using the LDA approach may be related to the use of the electron density of Si (Fig. 2), as was theoretically determined. At the same time, the ELF was obtained from the experimental data. Therefore, to avoid excessive information, in Figs. 5–11, we will present only the results based on the Penn approach.

The Penn approach, combined with the real-time TDDFT and IDA methods, provides accurate results that agree with the experimental data. The IDA-Penn results show excellent agreement at all the velocities shown in Fig. 4. Although IDA has shown excellent agreement with the experimental data, its use in electronic stopping

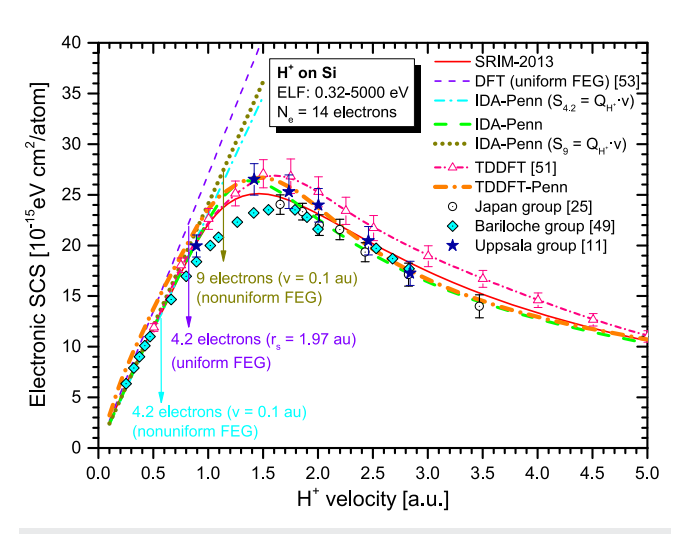


FIG. 5. As shown in Fig. 4, but in linear scale, electronic SCS for H $^+$ ions on Si is presented as a function of velocity. The IDA-Penn (green dashed line) and real-time TDDFT-Penn (orange short-dashed–dotted line) results are shown. For comparison, we plot the original uniform nonlinear DFT estimates (violet short-dashed line) for the proportional SCS to the velocity. SProportional SCS to the H $^+$ velocity ($S = Q \cdot v$), calculated from the IDA-Penn approach, is shown for two cases: the cyan dashed–dotted line is the result for 4.2 electrons per Si molecule contributing to the nonuniform FEG (see Fig. 3); the dark yellow short-dotted line is the result with full ELF, in which nine electrons effectively contribute to the nonuniform FEG in the electron–H $^+$ interaction.

power estimates for Z > 2 leads to underestimated results. For this reason, only the TCS results are presented for Z > 2 and $v \le 0.8$ a.u.

The real-time TDDFT results obtained from plane-wave pseudopotential calculations and scaled by a velocity-dependent factor to

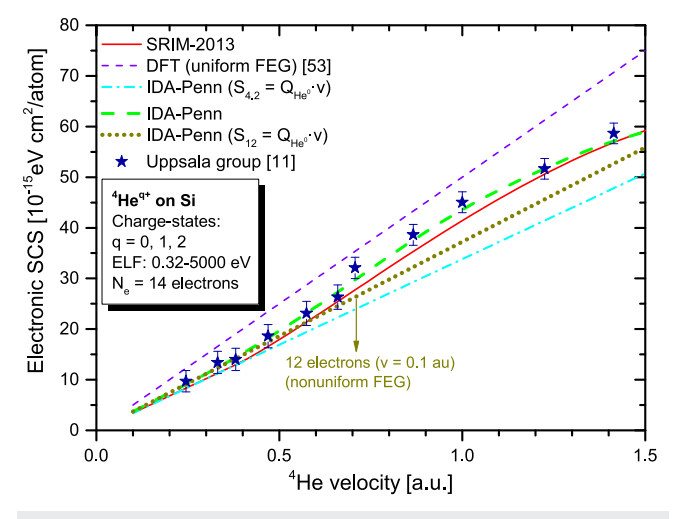


FIG. 6. Electronic SCS averaged over the charge states for He^{q+} ions on Si as a function of velocity. The IDA-Penn (green dashed line) results are compared to the original uniform nonlinear DFT estimates (short-dashed line),⁵³ proportional to the He^0 velocity. As shown in Fig. 5, IDA-Penn for the linear SCS is presented: the dark yellow short-dotted line is the result with full ELF, in which 12 electrons effectively contribute to the nonuniform FEG in electron— He^0 interaction.

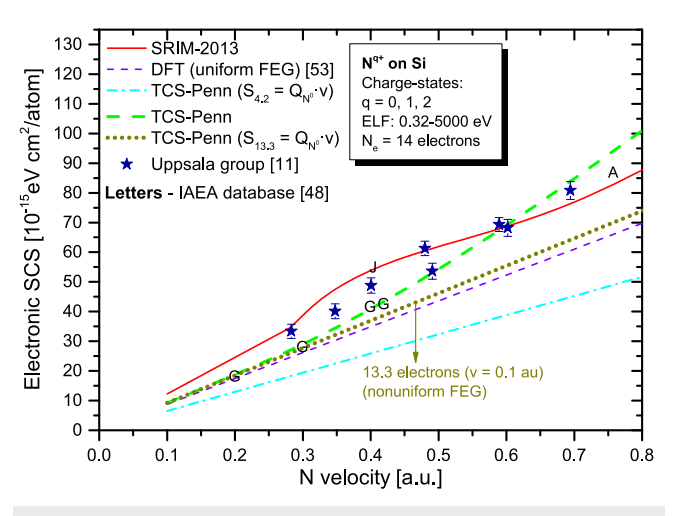


FIG. 7. As shown in Fig. 6, we present the electronic SCS averaged over the charge states for N^{q+} ions on Si as a function of velocity. TCS-Penn results (green dashed line) are shown. TCS-Penn results for the SCS proportional to the N⁰ velocity (IDA-Penn = TCS-Penn, for q = 0)^{7,8} are presented: the dark yellow short-dotted line is the result with full ELF, in which 13.3 electrons effectively contribute to the nonuniform FEG in electron-N⁰ interaction.

account for the absent core electrons⁵¹ agree with our results of IDA-LDA and TDDFT-LDA (Fig. 4) at $\nu > 2$ a.u. However, the results of Yost *et al.*⁵¹ show the stopping maximum shifted to higher velocity compared to our results, and below the maximum, it is closer to IDA-Penn and TCS-LDA.

In Fig. 5, we show the same as in Fig. 4 but in linear scale and including the original nonlinear DFT estimates to SCS, ⁵³ which are proportional to the H⁺ velocity, $dE/dz \equiv S = Q \cdot v$, where Q is a velocity-independent friction coefficient by Echenique *et al.*¹³

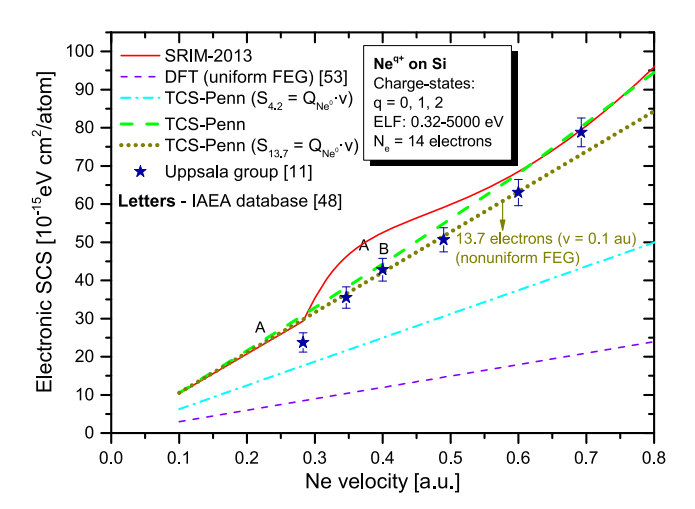


FIG. 8. As shown in Figs. 6 and 7, electronic SCS averaged over the charge states for Ne^{q+} ions on Si as a function of velocity is shown. TCS-Penn results for the linear SCS are presented: the dark yellow short-dotted line is the result with full ELF, in which 13.7 electrons effectively contribute to the nonuniform FEG in electron- Ne^0 interaction.

The DFT calculations for the friction coefficients are expected to agree with our calculations at $\nu \to 0$. Still, the velocity-proportional stopping extrapolation can overestimate or underestimate the stopping power for finite ion velocities. This will be important when we analyze the SCS for heavier ions at low velocities.

The predominant charge states for He, N, and Ne projectiles at $v < v_F$ are q = 0, 1 for He and q = 0, 1, 2, and 3 for N and Ne. Although the real-time TDDFT method is considered a benchmark, it was not used in calculating the electronic stopping of He, N, and Ne in Si because the current code considers only bare ions.⁴³

In Figs. 5–8, the proportional SCS to the He, N, and Ne velocity was determined from the values of the friction coefficient Q. Stopping power values were obtained using the IDA-Penn (for H^+ , H^0 , and He^0) and TCS-Penn (for N^0 and Ne^0) approaches at $\nu=0.1$ a.u. CasP 6.0 program⁵² shows that the projectiles have neutral charges at this speed. Therefore, we consider only the charge state $q=Z-n_b=0$, where n_b represents the number of electrons bound to the ion; as mentioned in Sec. II D, the IDA and TCS methods yield the same results for neutral projectiles:^{7,8} IDA-Penn(q=0) = TCS-Penn(q=0). The values of Q for H^+ , H^0 , He^0 , N^0 , and Ne^0 are 0.2337, 0.1958, 0.3612, 0.8959, and 1.0224 a.u., respectively.

The DFT results shown in Figs. 5–8 were obtained assuming a uniform FEG for the Si valence band.⁵³ We used an electron–gas parameter $r_{s,exp} = 1.97$ a.u. for this uniform FEG obtained from the experimental plasmon energy of Si.^{36,54} This r_s value was used in the DFT calculation, corresponding to 4.2 valence electrons.

The DFT results (violet short-dashed line) show that the assumption of uniformity in electron density fails for electronic SCS estimates of N and Ne in Si, as pointed out in the experimental work.¹¹

When considering the nonuniformity of electrons in the calculations of IDA-Penn (or TCS-Penn) using the (0.32 $\leq \omega \leq$ 100) eV range (4.2 electrons), as shown in Fig. 3, we determined the proportional SCS to the estimation of the velocity of neutral projectiles, as shown by the cyan dashed-dotted line in Figs. 5-8. The dark yellow short-dotted line represents the IDA-Penn (Figs. 5 and 6) and TCS-Penn (Figs. 7 and 8) results for the effective electrons in a nonuniform FEG. Therefore, based on the ranges shown in Fig. 3, we can draw the following conclusions: the calculations of IDA-Penn (or TCS-Penn) suggest that the H⁺ [or H⁰, see Fig. 9(a)] projectiles interact with a nonuniform FEG of nine electrons, which is higher than the prediction of 4.2 electrons (uniform FEG).³⁶ Similarly, the He⁰ projectiles interact with 12 electrons, while the N⁰ and Ne^{0} projectiles interact with ~13 electrons from Si. As the projectile nuclear charge increases, this discrepancy may stem from increased electron-hole pair excitations from the inner shells¹¹ However, this phenomenon is not adequately described in FEG-based models due to the absence of binding energy in the model, which rapidly decreases as the velocity approaches zero. Another notable phenomenon is the electron elevator mechanism observed in ab initio calculations for Si in Si, as discussed in Ref. 55, where excitations are present between energy gaps via a dynamical gap state.

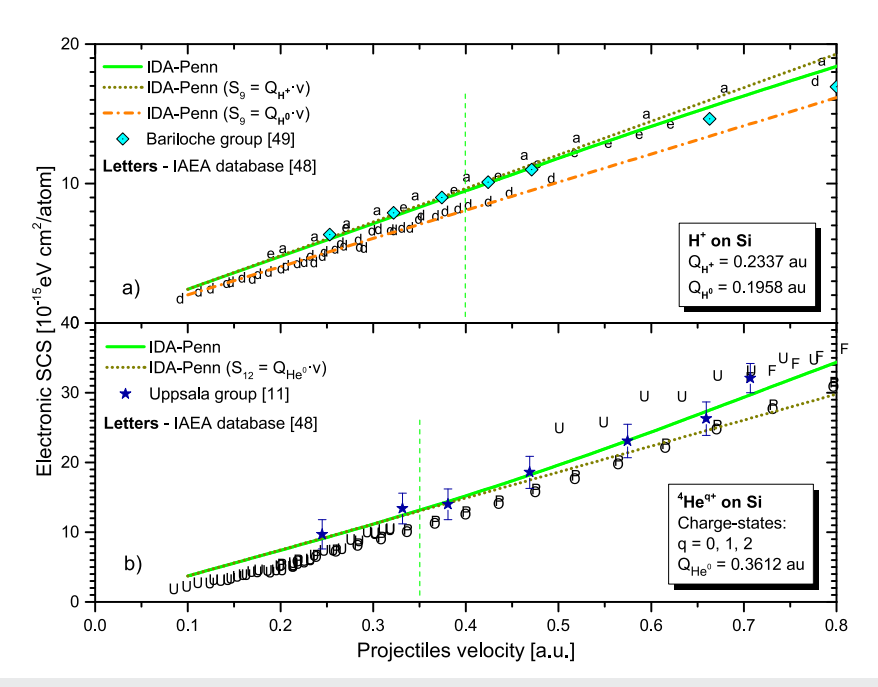


FIG. 9. Electronic SCS results for (a) H and (b) He calculated using the IDA-Penn approach. In panel (a), the green solid line is the result of the nonlinear SCS to the H⁺ velocity; the dark yellow short-dotted line is the result of the proportional SCS to the H⁺ velocity ($Q_{H^+} = 0.2337$ a.u.) performed at v = 0.1 a.u. The results of proportional SCS to the H⁰ velocity ($Q_{H^0} = 0.1958$ a.u.) are presented in an orange short-dashed–dotted line. The result for He is presented in panel (b): the green solid line is the result of the nonlinear SCS, and the dark yellow short-dotted line is the result of the proportional SCS to the He⁰ velocity ($Q_{H^0} = 0.3612$ a.u.). The letters are experimental data available at the IAEA database,⁴⁸ and the royal star symbols are the Uppsala group results.¹¹

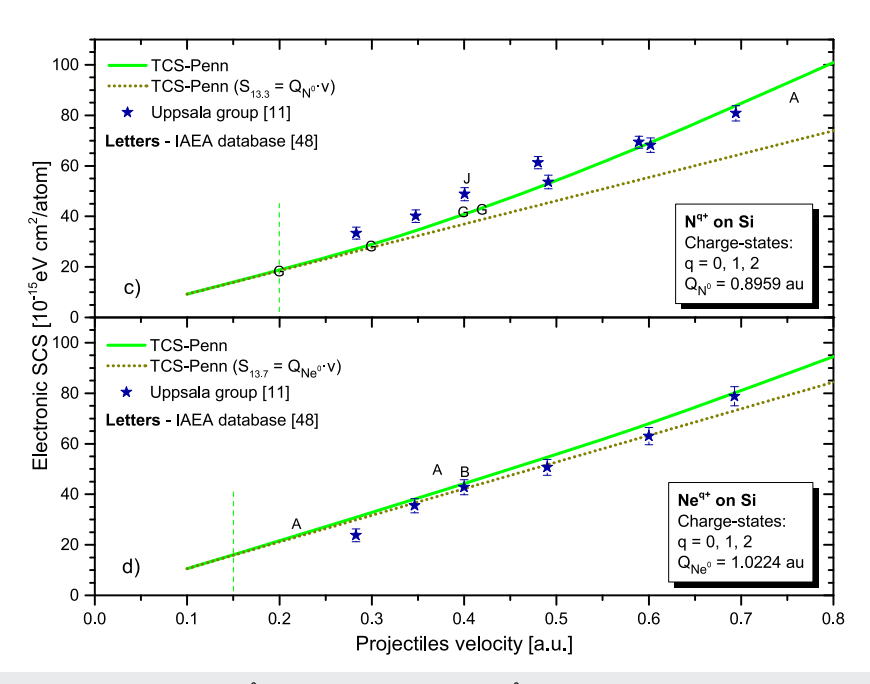


FIG. 10. As shown in Fig. 9(c), electronic SCS results for N⁰ ($Q_{N^0} = 0.8959$ a.u.) and (d) Ne⁰ ($Q_{Ne^0} = 1.0224$ a.u.) are presented, recalling the IDA-Penn = TCS-Penn for $q = 0.7^{.8}$

The nonlinear SCS results for He, N, and Ne are shown in Figs. 6–8, respectively. The IDA-Penn results (green dashed line) for He show an excellent agreement with the experimental data. 11,48

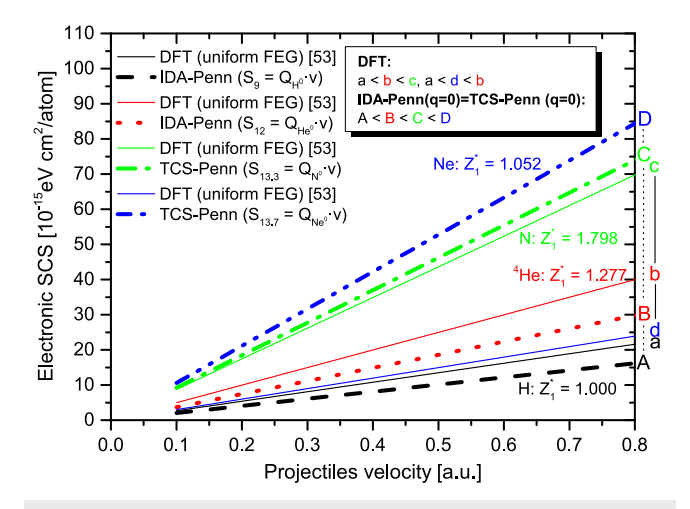


FIG. 11. Electronic SCS results for H⁰, He⁰, N⁰, and Ne⁰. The not-continuous lines are the results of the electronic stopping coefficient ($S = Q \cdot \nu$) performed in the IDA-Penn (or TCS-Penn) approach at $\nu = 0.1$ a.u.: H⁰ (black dashed line, letters A), He⁰ (red dotted line, letters B), N⁰ (green dashed–dotted line, letters C), and Ne⁰ (blue dashed–double-dotted line, letters D). The DFT results⁵³ are shown for comparison: H⁰ (black solid line, letters a), He⁰ (red solid line, letters b), N⁰ (green solid line, letters c), and Ne⁰ (blue solid line, letters d). Z₁* represents the effective charge values for each neutral atom.⁵³

The slope coefficient of the linear SCS (dark yellow short-dotted line) provided by IDA-Penn is much more accurate than the uniform nonlinear DFT results. It should be noted that this discrepancy does not come from nonlinear DFT but rather from the assumption of uniformity in the electron density. The results for Ne in Si have the greatest discrepancy between the results with uniform and nonuniform electron density, as shown in Fig. 8.

As evident in Figs. 5–8, the dependence of electronic stopping on the nonuniformity of the electron density increases as the atomic charge of the ion increases. The consequences of these effects will be discussed in relation to Figs. 9 and 10.

Figures 9 and 10 show the comparison between the nonlinear SCS and SCS proportional to the neutral projectile velocity, both calculated from the stopping coefficient, $S = Q \cdot v$; we calculate Q considering the value of the stopping power at v = 0.1 and then we extrapolate electronic stopping proportional to velocity for v > 0.1 a.u.

We note a velocity-proportionality breakdown in SCS that occurs at velocities of 0.40 [for H, Fig. 9(a)], 0.35 [for He, Fig. 9(b)], 0.20 [for N, Fig. 10(c)], and 0.15 a.u. [for Ne, Fig. 10(c)]. Moreover, we observe a pattern for these breaks: the SCS range (linear to velocity) decreases as the atomic charge of the ion increases. This indicates that the velocity range is influenced solely by weakly bound electrons from the valence band, which contribute to stopping and become narrower with increasing projectile charge. The uniform FEG approach fails to consider all potential excitations. Deeper electrons can be dynamically excited through alternative mechanisms, such as the "elevator" and/or "promotion," enabling physical scenarios where a localized free-electron gas can emulate ion energy loss. This localized free-electron gas describes how

electrons, although bound within localized regions, behave similarly to a free-electron gas when excited. This aligns with the observations of Refs. 11 and 55 Therefore, it is crucial to consider electron density nonuniformity in these calculations, as it significantly improves electronic stopping and allows for the emulation of effects beyond the simple electron-hole excitation.

In Fig. 11, an interesting result is presented, which is similar to Figs. 5-8 in terms of the DFT and IDA-Penn (or TCS-Penn) estimates. The uniform DFT results (solid lines) are presented for H⁰ (a), He⁰ (b), N⁰ (c), and Ne⁰ (d). On the other hand, the IDA-Penn results for the SCS proportional to the velocity of the neutral projectile are shown as A (H⁰), B (He⁰), C (N⁰), and D (Ne⁰).

In the uniform nonlinear DFT predictions, we observed a relationship between the inclinations of the SCS lines. In particular, we have found that a < b < c and a < d < b. The figure showing the SCS results also includes the effective charge values for each projectile.⁵³ It is worth noting that the effective charge values increase from H⁰ to N⁰, but the effective charge value of Ne⁰ is slightly higher than that of H⁰. These oscillations in effective charge values of the atoms are well known and can be confirmed in Fig. 15 of Ref. 53.

When we consider the nonuniform FEG and account for the inner shells' electron contributions, we notice that the slopes of the SCS lines increase as the ions' atomic charge increases. This nonuniformity of the electron density and the contributions of inner electrons to the SCS alter the slope pattern: A < B < C < D.

IV. CONCLUSIONS

Our findings emphasize on the importance of considering nonuniform electron density, shedding new light on local density approximations, particularly their ability to dynamically incorporate contributions from deeper-band electrons. Furthermore, we observe a breakdown in the proportionality relationship between stopping power and velocity as ν approaches zero. The higher the projectile charge, the lower the velocity at which this breakdown occurs. This phenomenon, explaining the findings observed in Ref. 11, probably arises from the possibility of dynamic changes in deep energy levels due to the "elevator" and/or "promotion" mechanisms. These mechanisms can create scenarios resembling a local free-electron gas.

Although the standard DFT approach proved inadequate for these calculations, a nonuniform DFT approach, or ideally full ab initio calculation, is expected to produce results consistent with the estimates of IDA-Penn/TCS-Penn for electronic stopping. Using a local density approximation contributes to a better understanding of the complexities in electron-ion interactions in this context.

ACKNOWLEDGMENTS

This study was financed in part by the IPEN (Project No. 2020.06.IPEN.32) and CNPq (Project No. 406982/2021-0), by the Coordenação de Aperfeiçoamento de Pessoal de Nível Superior -Brazil (CAPES) - Finance Code 001, by FINEP, by the Conselho Nacional de Desenvolvimento Científico e Tecnológico (CNPq), by the Instituto Nacional de Engenharia de Superfícies (INES) and PRONEX-FAPERGS. The authors acknowledge FAPESP for supporting the computer cluster (Process Nos. 2012/04583-8 and 2020/04867-2). T.F.S. acknowledges the financial support provided by CNPq-INCT-FNA (Project No. 464898/2014-5).

AUTHOR DECLARATIONS

Conflict of Interest

The authors have no conflicts to disclose.

Author Contributions

F. Matias: Conceptualization (equal); Methodology (equal); Software (equal); Validation (equal); Writing - original draft (equal). P. L. Grande: Methodology (equal); Validation (equal); Writing review & editing (equal). N. E. Koval: Data curation (equal); Writing - review & editing (equal). J. M. B. Shorto: Data curation (equal); Funding acquisition (equal); Writing - review & editing (equal). T. F. Silva: Funding acquisition (equal); Methodology (equal); Validation (equal); Writing - review & editing (equal). N. R. Arista: Methodology (equal); Validation (equal); Writing – review & editing (equal).

DATA AVAILABILITY

The data that support the findings of this study are available from the corresponding author upon reasonable request.

REFERENCES

- ¹J. M. Pruneda, D. Sánchez-Portal, A. Arnau, J. I. Juaristi, and E. Artacho, "Electronic stopping power in LiF from first principles," Phys. Rev. Lett. 99, 235501 (2007).
- ²M. Quijada, A. G. Borisov, I. Nagy, R. D. Muiño, and P. M. Echenique, "Timedependent density-functional calculation of the stopping power for protons and antiprotons in metals," Phys. Rev. A 75, 042902 (2007).
- ³D. Goebl, W. Roessler, D. Roth, and P. Bauer, "Influence of the excitation threshold of d electrons on electronic stopping of slow light ions," Phys. Rev. A 90, 042706 (2014).
- ⁴D. Roth, B. Bruckner, M. V. Moro, S. Gruber, D. Goebl, J. I. Juaristi, M. Alducin, R. Steinberger, J. Duchoslav, D. Primetzhofer, and P. Bauer, "Electronic stopping of slow protons in transition and rare earth metals: Breakdown of the free electron gas concept," Phys. Rev. Lett. 118, 103401 (2017).
- ⁵D. Roth, B. Bruckner, G. Undeutsch, V. Paneta, A. I. Mardare, C. L. McGahan, M. Dosmailov, J. I. Juaristi, M. Alducin, J. D. Pedarnig, R. F. Haglund, D. Primetzhofer, and P. Bauer, "Electronic stopping of slow protons in oxides: Scaling properties," Phys. Rev. Lett. 119, 163401 (2017).
- ⁶M. A. Sortica, V. Paneta, B. Bruckner, S. Lohmann, M. Hans, T. Nyberg, P. Bauer, and D. Primetzhofer, "Electronic energy-loss mechanisms for H, He, and Ne in TiN," Phys. Rev. A 96, 032703 (2017).
- $^{\bf 7}\text{P.}$ L. Grande, "Alternative treatment for the energy-transfer and transport cross section in dressed electron-ion binary collisions," Phys. Rev. A 94, 042704 (2016). ⁸F. Matias, R. C. Fadanelli, P. L. Grande, N. E. Koval, R. D. Muiño, A. G. Borisov, N. R. Arista, and G. Schiwietz, "Ground- and excited-state scattering potentials for the stopping of protons in an electron gas," J. Phys. B: At., Mol. Opt. Phys. 50, 185201 (2017).
- ⁹R. Ullah, E. Artacho, and A. A. Correa, "Core electrons in the electronic stopping of heavy ions," Phys. Rev. Lett. 121, 116401 (2018).
- ¹⁰M. A. Sortica, V. Paneta, B. Bruckner, S. Lohmann, T. Nyberg, P. Bauer, and D. Primetzhofer, "On the Z₁-dependence of electronic stopping in TiN," Sci. Rep. 9, 176 (2019).

- ¹¹E. Ntemou, S. Lohmann, R. Holeňák, and D. Primetzhofer, "Electronic interaction of slow hydrogen, helium, nitrogen, and neon ions with silicon," Phys. Rev. B **107**, 155145 (2023); Erratum, **109**, 239902 (2024).
- ¹²M. J. Puska and R. M. Nieminen, "Atoms embedded in an electron gas: Phase shifts and cross sections," Phys. Rev. B 27, 6121 (1983).
- ¹³P. M. Echenique, R. M. Nieminen, J. C. Ashley, and R. H. Ritchie, "Nonlinear stopping power of an electron gas for slow ions," Phys. Rev. A 33, 897 (1986).
- ¹⁴F. Matias, P. L. Grande, M. Vos, P. Koval, N. E. Koval, and N. R. Arista, "Nonlinear stopping effects of slow ions in a no-free-electron system: Titanium nitride," Phys. Rev. A 100, 030701(R) (2019).
- ¹⁵B. Gu, B. Cunningham, D. Muñoz Santiburcio, F. Da Pieve, E. Artacho, and J. Kohanoff, "Efficient *ab initio* calculation of electronic stopping in disordered systems via geometry pre-sampling: Application to liquid water," J. Chem. Phys. 153, 034113 (2020).
- ¹⁶ A. Kononov, T. Hentschel, S. Hansen *et al.*, "Trajectory sampling and finite-size effects in first-principles stopping power calculations," npj Comput. Mater. **9**, 205 (2023).
- ¹⁷F. Matias, T. F. Silva, N. E. Koval, J. J. N. Pereira, P. C. G. Antunes, P. T. D. Siqueira, M. H. Tabacniks, H. Yoriyaz, J. M. B. Shorto, and P. L. Grande, "Efficient computational modeling of electronic stopping power of organic polymers for proton therapy optimization," Sci. Rep. 14, 9868 (2024).
- ¹⁸T. L. Ferrell and R. H. Ritchie, "Energy losses by slow ions and atoms to electronic excitation in solids," Phys. Rev. B 16, 115 (1977).
- ¹⁹A. Cherubini and A. Ventura, "Stopping of light ions in homogeneous electron gases," Lett. Nuovo Cimento, Ser. 2 44, 503 (1985).
- ²⁰B. Apagyi and I. Nagy, "A simple calculation of the stopping power of an electron gas for slow protons," J. Phys. C: Solid State Phys. **20**, 1465 (1987).
- ²¹ J. Friedel, "XIV. The distribution of electrons round impurities in monovalent metals," London, Edinburgh Dublin Philos. Mag. J. Sci. 43, 153–189 (1952).
- ²²J. Friedel, "Electronic structure of primary solid solutions in metals," Adv. Phys. 3, 446–507 (1954).
- ²³ A. F. Lifschitz and N. R. Arista, "Velocity-dependent screening in metals," Phys. Rev. A 57, 200 (1998).
- ²⁴ A. F. Lifschitz and N. R. Arista, "Electronic energy loss of helium ions in aluminum using the extended-sum-rule method," Phys. Rev. A 58, 2168 (1998).
- ²⁵ A. Ikeda, K. Sumitomo, T. Nishioka, and Y. Kido, "Stopping powers and energy staggling for 50–300 keV H⁺ in amorphous Si and Ge films," Nucl. Instrum. Methods Phys. Res., Sect. B **115**, 34–38 (1996); part of Special Issue: Atomic Collisions in Solids.
- ²⁶N. Arista, "Energy loss of ions in solids: Non-linear calculations for slow and swift ions," Nucl. Instrum. Methods Phys. Res., Sect. B 195, 91–105 (2002).
- ²⁷J. Lindhard and M. Scharff, Mat.-Fys. Medd.-K. Dan. Vidensk. Selsk. 27, 15 (1953).
- ²⁸E. Bonderup, Mat.-Fys. Medd.-K. Dan. Vidensk. Selsk. 35, 17 (1967).
- ²⁹E. Bonderup and P. Hvelplund, "Stopping power and energy straggling for swift protons," Phys. Rev. A **4**, 562 (1971).
- ³⁰C. C. Rousseau, W. K. Chu, and D. Powers, "Calculations of stopping cross sections for 0.8- to 2.0-MeV alpha particles," Phys. Rev. A 4, 1066–1070 (1971).
- ³¹ J. Calera-Rubio, A. Gras-Marti, and N. R. Arista, "Stopping power of low-velocity ions in solids: Inhomogeneous electron gas model," Nucl. Instrum. Methods Phys. Res., Sect. B 93, 137–141 (1994).
- ³²D. R. Penn, "Electron mean-free-path calculations using a model dielectric function," Phys. Rev. B 35(2), 482–486 (1987).
- ³³H. Shinotsuka, S. Tanuma, C. Powell, and D. Penn, "Calculations of electron stopping powers for 41 elemental solids over the 50 eV to 30 keV range with the full Penn algorithm," Nucl. Instrum. Methods Phys. Res., Sect. B **270**, 75–92 (2012).

- ³⁴ M. Vos and P. Grande, "Extension schemes of the dielectric function, and their implications for ion stopping calculations," J. Phys. Chem. Solids 133, 187–196 (2019).
- ³⁵J. Ziegler, J. Biersack, and U. Littmark, in *The Stopping and Range of Ions in Solids*, edited by J. F. Ziegler (Pergamon Press, Inc., 1985), Vol. 1.
- ³⁶A. Mann and W. Brandt, "Material dependence of low-velocity stopping powers," Phys. Rev. B **24**, 4999–5003 (1981).
- ³⁷S. Tanuma, C. Powell, and D. Penn, "Use of sum rules on the energy-loss function for the evaluation of experimental optical data," J. Electron Spectrosc. Relat. Phenom. 62, 95–109 (1993).
- ³⁸A. G. Borisov, J. P. Gauyacq, and S. V. Shabanov, "Wave packet propagation study of the charge transfer interaction in the F-Cu(111) and -Ag(111) systems," Surf. Sci. **487**, 243–257 (2001).
- ³⁹ A. G. Borisov, J. I. Juaristi, R. D. Muiño, D. Sánchez-Portal, and P. M. Echenique, "Quantum-size effects in the energy loss of charged particles interacting with a confined two-dimensional electron gas," Phys. Rev. A 73, 012901 (2006).
- ⁴⁰E. V. Chulkov, A. G. Borisov, J. P. Gauyacq, D. Sánchez-Portal, V. M. Silkin, V. P. Zhukov, and P. M. Echenique, "Electronic excitations in metals and at metal surfaces," Chem. Rev. 106, 4160–4206 (2006).
- ⁴¹ M. Quijada, R. Díez Muiño, A. G. Borisov, J. A. Alonso, and P. M. Echenique, "Lifetime of electronic excitations in metal nanoparticles," New J. Phys. 12, 053023 (2010).
- ⁴²N. E. Koval, D. Sánchez-Portal, A. G. Borisov, and R. D. Muiño, "Dynamic screening of a localized hole during photoemission from a metal cluster," Nanoscale Res. Lett. 7, 447 (2012).
- ⁴³N. E. Koval, D. Sánchez-Portal, A. G. Borisov, and R. Díez Muiño, "Dynamic screening and energy loss of antiprotons colliding with excited Al clusters," Nucl. Instrum. Methods Phys. Res., Sect. B 317, 56–60 (2013).
- ⁴⁴A. Borisov, D. Sánchez-Portal, R. Díez Muiño, and P. Echenique, "Building up the screening below the femtosecond scale," Chem. Phys. Lett. 387, 95–100 (2004).
- ⁴⁵J. Finnemann, "En redegørelse for resultaterne af beregninger over spredning af elektroner med lav energi p afskærmede coulombfelter," M.Sc. thesis, Aarhus University, 1968.
- 46 J. Briggs and A. Pathak, "Momentum transfer cross sections and the Z₁ oscillations in stopping power," J. Phys. C: Solid State Phys. 6, L153 (1973).
- ⁴⁷P. Sigmund, Particle Penetration and Radiation Effects (Springer, Berlin, 2006), Vol. 1, p. 151.
- ⁴⁸IAEA Stopping Power Database, "Electronic stopping power of matter for ions," available from https://nds.iaea.org/stopping (version 2024-03).
- ⁴⁹M. Famá, G. Lantschner, J. Eckardt, N. Arista, J. Gayone, E. Sanchez, and F. Lovey, "Energy loss and angular dispersion of 2–200 keV protons in amorphous silicon," Nucl. Instrum. Methods Phys. Res., Sect. B 193, 91–96 (2002).
- ⁵⁰ J. F. Ziegler, M. Ziegler, and J. Biersack, "SRIM—The stopping and range of ions in matter," Nucl. Instrum. Methods Phys. Res., Sect. B 268, 1818–1823 (2010).
- ⁵¹ D. C. Yost, Y. Yao, and Y. Kanai, "Examining real-time time-dependent density functional theory nonequilibrium simulations for the calculation of electronic stopping power," Phys. Rev. B 96, 115134 (2017).
- ⁵²P. L. Grande and G. Schiwietz, "Convolution approximation for swift particles (CASP) program," free download from http://www.casp-program.org, 2021.
- ⁵³P. Echenique, F. Flores, and R. Ritchie, "Dynamic screening of ions in condensed matter," Solid State Phys. **43**, 229–308 (1990).
- 54 D. Isaacson, "Compilation of $r_{\rm s}$ values," Doc. No. 02698, Radiation and Solid State Laboratory New York University, 1975.
- ⁵⁵A. Lim, W. M. C. Foulkes, A. P. Horsfield, D. R. Mason, A. Schleife, E. W. Draeger, and A. A. Correa, "Electron elevator: Excitations across the band gap via a dynamical gap state," Phys. Rev. Lett. 116, 043201 (2016).